become through other processes, conduits for surficial runoff. On Earth, both sapping and piping occur together with other processes that operate to remove their debris products. Without such removal, the groundwater processes choke in their own detritus. In terrestrial desert settings, flash floods are essential to removing the accumulated products (*48*). Where the eroding bedrock is sandstone, wind transport also plays an important role in removing debris.

33. C. G. Higgins *et al.*, *Geol. Soc. Am. Spec. Pap. 252* (1990), pp. 139–155.
34. It is difficult to reconcile the environments where the gullies are observed with an origin requiring liquid water because of the cold temperatures and low atmospheric pressures. Being polar and subpolar, these features spend as much as half a martian year at or near the freezing point of carbon dioxide (at martian pressures, ~148 K), or nearly 125 K below the triple point of water. Further, they occur on predominantly poleward-facing slopes, which are subject to substantially lower solar insolation and hence lower temperatures at any given latitude than the insolation and temperatures of adjacent flat, east/west, or equator-facing slopes. Most gullies occur in the southern hemisphere, which has a relatively high elevation, and hence at lower atmospheric pressure (increasing the evaporation rate).
35. The only exceptions are the gullies in the south- and southeast-facing walls of Dao Vallis, which heads within and follows a course though materials associated with the ancient highland volcano, Hadriaca Patera.
36. An estimate of the minimum amount of water that may have participated in the formation of the gullies can be made as follows. We assume that the aprons were formed primarily by debris flows. Field and laboratory measurements [e.g., (*49, 50*)] indicate that such flows contain no less than 10% by volume water and typically no more than 30% by volume (little or no mobility occurs with lower water content; higher water content leads to mudflows or hyperconcentrated stream flow). Aprons vary substantially in area; those seen in Fig. 5 cover ~1.25 million square meters. Assuming a thickness of ~2 m and a volume fraction of 10% leads to a water volume of 250,000 m^3 (250 million liters or 66 million gallons). For reference, if fully accessible, this would be enough water to supply 100 people for nearly 20 years (without recycling). About 100 channels feed these aprons, suggesting that each apron-forming event involves 2500 m^3 (2.5 million liters or 660,000 gallons) of water, enough for 20 people for a year. Factors that would reduce the amount of water include evaporation and/or sublimation of the water after emplacement; factors that may increase the amount include greater apron thickness and higher water volume fractions.
37. A. Albee, *Eos* **77** (no. 45), 441 (1996).
38. A. L. Albee *et al.*, *Science* **279**, 1671 (1998).
39. M. C. Malin *et al.*, *J. Geophys. Res.* **97**, 7699 (1992).
40. K. S. Edgett and M. C. Malin, *J. Geophys. Res.* **105**, 1623 (2000).
41. J. R. Zimbelman, *Geophys. Res. Lett.* **27**, 1069 (2000).
42. A. L. Washburn, *Geol. Soc. Am. Bull.* **67**, 823 (1956).
43. R. F. Black, *Quat. Res.* **6**, 3 (1976).
44. A. H. Lachenbruch, *Geol. Soc. Am. Spec. Pap. 70* (1962).
45. C. G. Higgins, in *Groundwater as a Geomorphic Agent*, R. G. LaFleur, Ed. (Allen & Unwin, Boston, 1984), pp. 18–58.
46. G. G. Parker Sr. *et al.*, *Geol. Soc. Am. Spec. Pap. 252* (1990), pp. 77–110.
47. R. B. Bryan and J. A. A. Jones, *Geomorphology* **20**, 209 (1997).
48. J. E. Laity and M. C. Malin, *Geol. Soc. Am. Bull.* **96**, 203 (1985).
49. J. Fink *et al.*, *Geophys. Res. Lett.* **8**, 43 (1981).
50. C. J. Kafura, thesis, Arizona State University, Tempe (1988).
51. The authors express their appreciation to M. Caplinger, E. Jensen, S. Davis, W. Gross, D. Michna, J. Sandoval, K. Supulver, and J. Warren for their efforts in support of the MOC. Without their hard work and dedication, the images on which this work is based would not have been acquired. W. Dietrich provided early guidance to consideration of the origin of the landforms described here. Comments by two anonymous referees provided useful perspectives on our results. This work was supported by Jet Propulsion Laboratory contracts 959060 and 1200780.

3 April 2000; accepted 16 May 2000

Microrobots for Micrometer-Size Objects in Aqueous Media: Potential Tools for Single-Cell Manipulation

Edwin W. H. Jager,* Olle Inganäs, Ingemar Lundström

Conducting polymers are excellent materials for actuators that are operated in aqueous media. Microactuators based on polypyrrole-gold bilayers enable large movement of structures attached to these actuators and are of particular interest for the manipulation of biological objects, such as single cells. A fabrication method for creating individually addressable and controllable polypyrrole-gold microactuators was developed. With these individually controlled microactuators, a micrometer-size manipulator, or microrobotic arm, was fabricated. This microrobotic arm can pick up, lift, move, and place micrometer-size objects within an area of about 250 micrometers by 100 micrometers, making the microrobot an excellent tool for single-cell manipulation.

The development of tools for the manipulation of single cells is of major importance for the rapidly growing area of genomics and proteomics, particularly in massively parallel single-cell manipulation and characterization. Actuators for the positioning and moving of objects such as cells must be compatible with the living conditions for cells. Optical tweezers fulfill some of these criteria, but they are not suited to massively parallel characterization; field cages (*1*) offer both possibilities. Here, we demonstrate an alternative in the form of a microrobotic arm operating in an aqueous environment, with dimensions suitable and scalable for the manipulation of cells. Our microfabricated devices are built on conjugated polymers used as the active element of a bending bilayer, which generates large-amplitude motion. Patterning of active and passive elements defines the geometry of a microrobot, whose individual bending beams are addressed separately and are therefore capable of more complex motions. We demonstrate the gripping and positioning of 100-μm objects with this microrobotic arm.

The term "microrobot" is often used for centimeter-size miniature robots built by conventional methods, combined with microelectronics for control. In our view, microrobots are millimeter and submillimeter devices with individual parts of micrometer size built by micromachining technology. Parts for such microrobots include hollow triangular robot links made of polycrystalline silicon (polysilicon) (*2*), in which systems of rods and levers are used to rotate the links out of plane of a substrate; wings for artificial flying insects based on polysilicon plates attached to polyimide hinges (*3*); and polysilicon microgrippers (*4*). An example of a complete microrobot is the walking silicon microrobot (*5*). The actuation here is based on the thermal expansion of polyimide deposited in V-shaped grooves etched in silicon with integrated heaters. However, none of these operate in water, and they would not be suitable as microactuators for the manipulation of cells.

Conducting polymers like polypyrrole (PPy) and polyaniline are excellent materials for actuators. Both macro- (*6–10*) and microactuators (*11–14*) based on these materials have been presented in the literature. These actuators are based on the reversible volume change of the conducting polymers upon oxidation and reduction. For the microactuators, we normally use PPy(DBS) (polypyrrole doped with dodecyl benzene sulfonate ions) in a bilayer configuration with Au acting as both a structural layer and an electrode. When we apply a negative potential on the Au (−1 V versus Ag/AgCl), we reduce the PPy to its neutral state [PPy^0 (Na^+DBS^-)]. To maintain charge neutrality,

Department of Physics and Measurement Technology, Division of Applied Physics, Linköpings universitet, S-581 83, Linköping, Sweden.

*To whom correspondence should be addressed. E-mail: edjag@ifm.liu.se

cations diffuse into the PPy from an ion source or sink (in our case, a NaDBS electrolyte solution), and the material swells. When we apply a positive potential (≥0 V), we oxidize the PPy [$PPy^+(DBS^-)$]. The cations now move out of the PPy back into the electrolyte, and the material shrinks. If we combine PPy in a bilayer configuration with Au (which does not change volume because of the applied potentials), the swelling and shrinking of the polymer results in a bending motion.

We have previously presented microactuators, also named "micromuscles," based on the PPy(DBS)/Au bilayer system. The microactuators were used to lift plates and to open and close boxes (*12*). The latter devices had three consecutive PPy/Au hinges in a row, which were operated simultaneously. However, a robotic arm needs individually addressable joints, which required some modifications of the previous design. First, we needed an insulating substrate. We chose to use a thermally oxidized Si wafer. The individual controllability also requires separate Au electrodes for each joint. The electrodes are mechanically connected through rigid parts made of benzocyclobutene (BCB) (Cyclotene 4024-40, Dow Chemical, Midland, Michigan). This causes BCB to be in contact with the substrate, and therefore, we cannot use the differential adhesion method (*15*). This method is based on the poor adhesion of Au on Si, but as BCB, which adheres well on Si, comes into contact with Si, the structures will stick to the substrate and release will be impossible. Therefore, we used a sacrificial layer.

Our robot arms consist of an elbow, a wrist, and a hand with fingers. The joints are mechanically connected by stiff elements of BCB. The wrist and elbow joints consist of two PPy/Au microactuators, each placed symmetrically around the upgoing electrical wires. We made two designs: one in which these two actuators are electrically connected to the same contact pad and one in which they have separate contact pads and thus can be separately addressed. We fabricated robots with varying numbers (two to four) and layout of the fingers, 10- or 20-μm wires, and fingers with and without rigid elements at the end.

A thermally evaporated, 500 to 700 Å Ti layer on an oxidized Si wafer was used as a sacrificial layer. We patterned this layer by using standard photolithographic techniques (Fig. 1A). Onto this layer, a 30 Å Cr adhesion layer and a structural layer of 1300 to 2100 Å Au were thermally evaporated. Next, slits were etched into the Cr/Au (Fig. 1B). These slits separated the electrodes/actuators. We only etched the slits and not the complete electrode/actuator layout because we wanted to keep the Au layer intact as long as possible. With the Au layer still intact at the PPy deposition step, we were able to grow PPy on all actuators simultaneously. Hereafter, we deposited the 2.1-μm BCB layer by photopolymerization. The BCB forms the rigid parts and connects the individual actuators (Fig. 1C). A 0.9- to 1.5-μm layer of PPy was electropolymerized from a 0.1 M NaDBS and 0.1 M pyrrole monomer solution at a voltage of 0.55 V versus Ag/AgCl. Before the deposition, the Au was masked with photoresist to pattern the PPy. The PPy grew on the parts of the Au that were not covered with photoresist. The result after the photoresist was removed is shown in Fig. 1D.

Next, the robots were released. A photoresist pattern with the layout of the robots, electrical wiring, and contact pads was deposited. We gave the resist a hard bake for 20 min at 110°C. The resist pattern was 5 μm longer and wider than the PPy structures to protect the PPy from the Au, Cr, and Ti etchants. We etched the Au and Cr and underetched the sacrificial Ti layer. Finally, we removed the photoresist with ethanol, and the robots were released, ready to be activated.

In the present layout, 140 microrobots were fabricated simultaneously on a quarter of a 10-cm Si wafer. After fabrication, we diced the wafer. A dice with a few robots was submerged in 0.1 M NaDBS electrolyte. We used an Au wire as a counter electrode and an Ag/AgCl electrode as a reference. All potentials mentioned are versus Ag/AgCl. We contacted the actuators using Au-coated probe tips (Karl Suss, Munich, Germany). To electrochemically control the microactuators, we used a custom-modified potentiostat, AutoLab PGSTAT10 (EcoChemie, Utrecht, Netherlands), with five extra working electrodes, giving us a total of six individually controlled working electrodes versus one counter electrode and one reference. The movement of the microrobot was recorded with a long working distance microscope and a video camera connected to a recorder. Pictures were taken using a frame grabber.

We started to activate the robots by running cyclic voltammetry (a triangular wave potential) on all joints simultaneously. We ran 5 to 10 cycles from 0 to −1.0 V at 100 mV/s to activate the PPy/Au bilayers to their maximum range. Hereafter, we individually controlled the actuators. By applying a voltage V between 0.2 and −1.0 V, we could control the bending of each joint at any angle. For instance, to grab a glass bead (as shown in Fig. 2B), we applied 0.2 V at

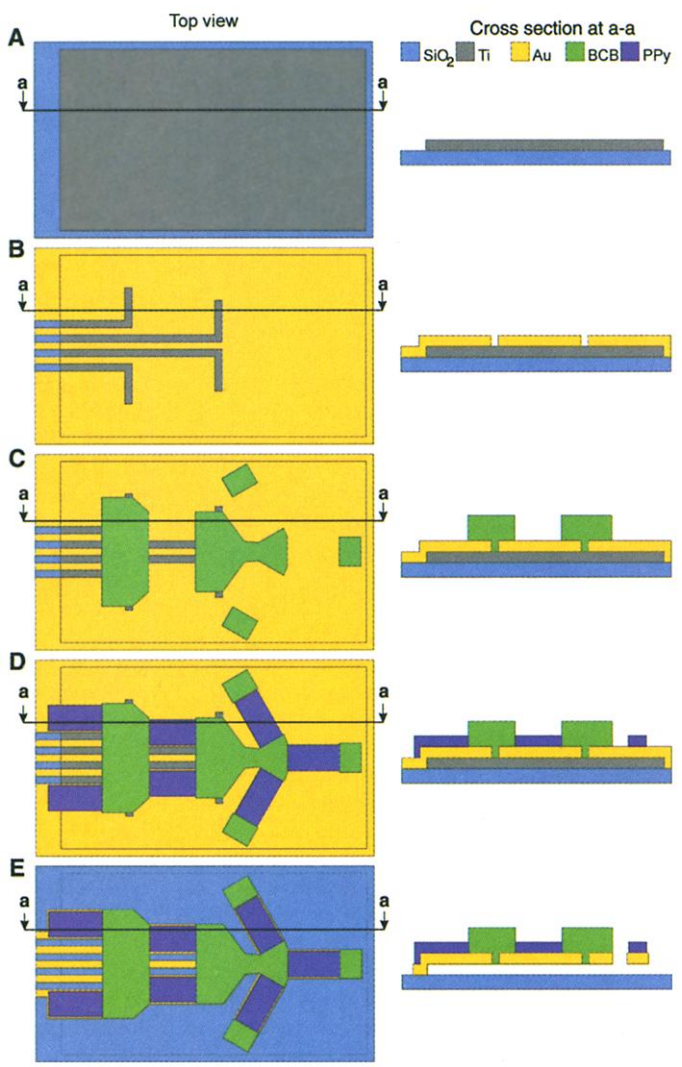

Fig. 1. A schematic drawing of the process steps for fabricating the microrobotic arms (in this case, an arm with three fingers). **(A)** Deposition and patterning of the sacrificial Ti layer. **(B)** Deposition of the structural Au layer and etching of the isolating slits. **(C)** Patterning of the BCB rigid elements. **(D)** Electrodeposition of PPy. **(E)** Etching of the final robot and electrode structure, removal of the sacrificial layer. Each microactuator is 100 μm by 50 μm. The total length of the robot is 670 μm, and the width at the base is either 170 or 240 μm (depending on the wire width, which was either 10 or 20 μm, respectively).

the elbow joint and −0.7 V at the wrist joint and fingers. We also applied a constant potential at some microactuators and a variable potential (running cyclic voltammetry) at the others. For instance, we lifted the arm perpendicular to the surface (V_{elbow} = −0.4 V, ~90° bent; V_{wrist} = −0.7 V, ~0° straight) and then opened and closed the fingers cyclically (*16*).

A sequence of pictures (Fig. 2) shows the lifting and displacement of a 100-μm glass bead (*16*). First, we moved the arm with opened fingers on top of the glass bead. Then, we closed the fingers to grab the glass bead, lifted it from the surface, moved the arm completely perpendicular to the surface (shown in gray), and then positioned the hand at the base of the robot arm. Here, we opened the fingers to release the bead and retracted the arm completely. The bead had been moved over a distance of 200 to 250 μm.

The robot arm with five contact pads also gave us individual control over the left and right actuator in the wrist and elbow joints. When we set a different potential to the left and right actuator, bending one and stretching the other, we achieved a minor sideways bending or rotation of ~20° of the arm, which further increased the operation range of the arm (*16*).

To further demonstrate the capabilities of the robot arm, we constructed tracks of polyurethane using MIMIC (micromolding in capillaries) (*17*) to simulate a conveyor belt system. We made a poly(dimethylsiloxane) (PDMS) (Sylgard, 184, Dow Corning, Midland, Michigan) mold from a master template made of the thick film photoresist SU-8. We then aligned the PDMS mold between the robot and the contact pads, with the tracks perpendicular to the electrical wiring. Next, we poured polyurethane prepolymer at one side of the mold and let the channels (10 to 11 mm long) fill by capillary action. We cured the polyurethane with ultraviolet light, peeled off the mold, and gave the polyurethane a short second cure. The result was a track system formed by 20-μm-high by 20-μm-wide polyurethane ribbons, 60 μm apart. We have also used thin freestanding PDMS films to fabricate the tracks. Although it is faster to make the tracks out of thin PDMS films, the alignment is more troublesome.

We placed a 100-μm glass bead at track number 4. Using the robot arm, we then moved it sequentially all over the tracks, from track 4 to 2, to 1, and to 3 and from the tracks to the base of the robot (Fig. 3) (*16*). In between, the bead was lifted from the substrate when we retracted the arm (Fig. 3D). The distance between the tracks was 60 μm, and the total displacement of the bead was 270 μm.

The PPy/Au micromuscles can be operated in salt solutions, blood plasma, urine, and cell culture medium; therefore, we think that our microrobots are most interesting for operations in biological fluids. In medicine, the robot could be used as a tool for minimal invasive surgery. A small robot put on a catheter would increase the range of the surgeon. Other applications of these microrobots

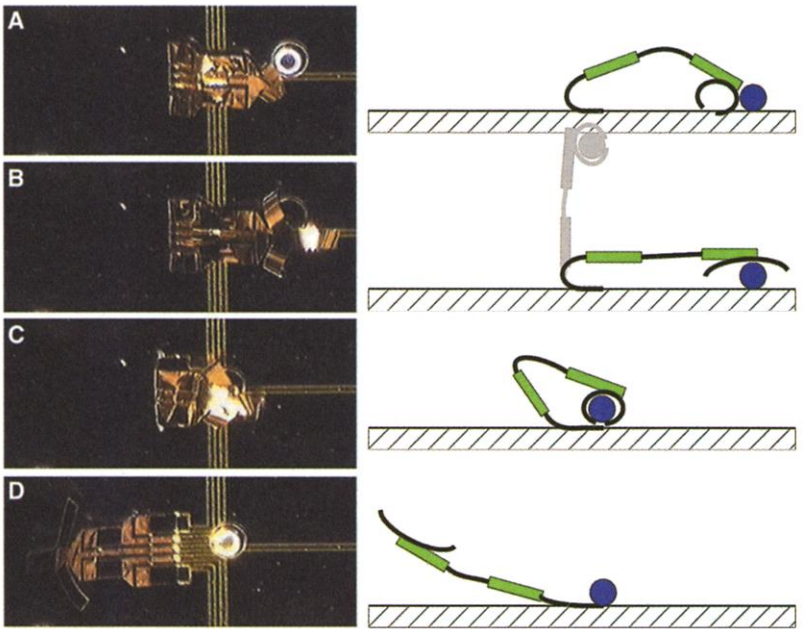

Fig. 2. (**A** through **D**) A sequence of pictures (left) showing the grabbing and lifting of a 100-μm glass bead and schematic drawings of the motion (right). In this case, the arm has three fingers, placed at 120° from each other. The pictures do not illustrate the fact that the bead is actually lifted from the surface before it is placed at the base of the robot arm. We have illustrated this in gray in the second sketch to the right. A film showing the full movement can be seen online (*16*).

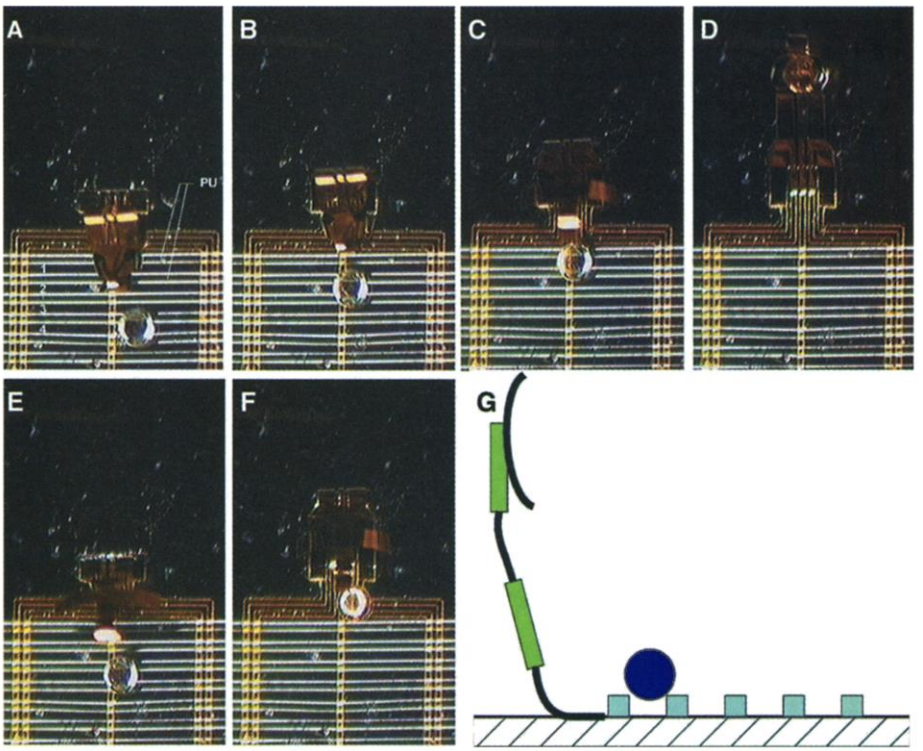

Fig. 3. (**A** through **F**) Picture sequence of moving a 100-μm glass bead over a polyurethane track system (*16*). The distance between two tracks is 60 μm. We picked up the glass bead and moved it from track 4 to 2, to 1, and to 3, and finally to the base of the robot outside of the tracks. The total maximum displacement of the glass bead was ~270 μm. In this case, the robot had three fingers placed at 90° from each other. In (D), the robot arm is fully retracted with the glass bead held in its fingers. (**G**) Schematic of the experimental layout.

include the "lab-on-a-chip" concept. The robots could be used for multistation single-cell diagnostics. The robot arm could arrest biological entities (single cells, bacteria, multicellular organisms, etc.) from a sample and then transfer them sequentially to different measurement stations of a multisensor area, as demonstrated by the transfer of the glass bead over the tracks. An array of standing microrobots, whose fingers are treated with adhesion molecules, could be used to select given cells or bacteria in a sample and then transfer them to the multisensor area. The testing could also be done by small additional structures on the microrobot itself, such as extra electrodes for electrical measurements. The electrodes could also be located on the chip itself, for example, in microvials, which also enable single-cell chemical modifications.

A nonbiomedical application for microrobots is the assembly of microstructures in a so-called "factory on a desk." The microrobot could be used to assemble other microstructures. Most of this is still done manually, which is cumbersome, time-consuming, and expensive. Small micromachined conveyors for this purpose have already been demonstrated (*18, 19*). An advantage of assembly in water could be the reduction of gravitational forces and slow diffusion constants of the objects to assemble. The robot could assist the self-assembly (*20*).

Design for the manipulation of cells will require choosing the proper dimensions of the microrobot. The simple scalability of the presented robots—they can easily be reduced in lateral dimension by one order of magnitude—is an important advantage. Also, our microactuators can be seen as active hinges, where only one electrical contact is needed per element, reducing the amount of dead area on the chip. This leads to the possibility of a large number of parallel-operated microrobots on a small area for the simultaneous handling of a large number of cells. Electrostatically operated microactuators require a considerable area for ingenious but complex systems using comb drive actuators and push or pull rods to rotate a plate out of the surface plane. To extend the range of the robot, some modifications of the present design should be made, like adding a rotating base. Using on-chip counter and working electrodes (*21*) would truly integrate the robot into a microelectromechanical system. The operation of such devices may enable new methods in biotechnology.

References and Notes

1. G. Fuhr and S. G. Shirley, *J. Micromech. Microeng.* **5**, 77 (1995).
2. R. Yeh, E. J. J. Kruglick, K. S. J. Pister, *J. Microelectromech. Syst.* **5**, 10 (1996).
3. K. Suzuki, I. Shimoyama, H. Miura, *J. Microelectromech. Syst.* **3**, 4 (1994).
4. C.-J. Kim, A. P. Pisano, R. S. Muller, *J. Microelectromech. Syst.* **1**, 31 (1992).
5. T. Ebefors, J. U. Mattsson, E. Kälvesten, G. Stemme, in *The 10th International Conference on Solid-State Sensors and Actuators, Digest of Technical Papers*, M. Esashi, Ed. (Institute of Electrical Engineers of Japan, Tokyo, 1999), pp. 1202–1205.
6. R. H. Baughman, L. W. Shacklette, R. L. Elsenbaumer, E. J. Plichta, C. Becht, in *Molecular Electronics*, P. I. Lazarev, Ed. (Kluwer Academic, Dordrecht, Netherlands, 1991), pp. 267–289.
7. T. F. Otero and J. M. Sansinena, *Proc. SPIE Int. Soc. Opt. Eng.* **2779**, 365 (1996).
8. A. Della Santa, D. De Rossi, A. Mazzoldi, *Smart Mater. Struct.* **6**, 23 (1997).
9. M. R. Gandhi, P. Murray, G. M. Spinks, G. G. Wallace, *Synth. Met.* **73**, 247 (1995).
10. Q. Pei and O. Inganäs, *Adv. Mater.* **4**, 277 (1992).
11. E. Smela, O. Inganäs, Q. Pei, I. Lundström, *Adv. Mater.* **5**, 630 (1993).
12. E. Smela, O. Inganäs, I. Lundström, *Science* **268**, 1735 (1995).
13. E. W. H. Jager, E. Smela, O. Inganäs, I. Lundström, *Proc. SPIE Int. Soc. Opt. Eng.* **3669**, 377 (1999).
14. E. Smela, *J. Micromech. Microeng.* **9**, 1 (1999).
15. ———, O. Inganäs, I. Lundström, in *The 8th International Conference on Solid-State Sensors and Actuators, and Eurosensors IX, Digest of Technical Papers* (Royal Swedish Academy of Engineering Sciences, Stockholm, 1995), pp. 218–219.
16. A film showing the full movement of this sequence and other actuations of the robotic arm is available at www.sciencemag.org/feature/data/1050465.shl.
17. Y. Xia and G. M. Whitesides, *Angew. Chem. Int. Ed. Engl.* **37**, 550 (1998).
18. H. Nakazawa *et al.*, in *The 10th International Conference on Solid-State Sensors and Actuators, Digest of Technical Papers*, M. Esashi, Ed. (Institute of Electrical Engineers of Japan, Tokyo, 1999), pp. 1192–1195.
19. Y. Mita, T. Oba, M. Mita, G. Hashiguchi, H. Fujita, in *The 10th International Conference on Solid-State Sensors and Actuators, Digest of Technical Papers*, M. Esashi, Ed. (Institute of Electrical Engineers of Japan, Tokyo, 1999), pp. 1196–1197.
20. T. L. Breen, J. Tien, S. R. J. Oliver, T. Hadzic, G. M. Whitesides, *Science* **284**, 948 (1999).
21. E. W. H. Jager, E. Smela, O. Inganäs, *Sens. Actuators B Chem.* **56**, 73 (1999).

22. E.W.H.J. is a Ph.D. student in the graduate school Forum Scientum and thanks the Swedish Foundation for Strategic Research (SSF) for its financial support. The micromuscle project is supported by the Swedish Research Council for Engineering Sciences (TFR).

16 March 2000; accepted 2 May 2000

Fractional Quantum Hall Effect in Organic Molecular Semiconductors

J. H. Schön, Ch. Kloc, B. Batlogg

High-quality crystals of the organic molecular semiconductors tetracene and pentacene were used to prepare metal-insulator-semiconductor (MIS) structures exhibiting hole and electron mobilities exceeding 10^4 square centimeters per volt per second. The carrier concentration in the channel region of these ambipolar field-effect devices was controlled by the applied gate voltage. Well-defined Shubnikov–de Haas oscillations and quantized Hall plateaus were observed for two-dimensional carrier densities in the range of 10^{11} per square centimeter. Fractional quantum Hall states were observed in tetracene crystals at temperatures as high as ~2 kelvin.

The quantum Hall effect (QHE) (*1*), in which the Hall resistance R_{xy} of a quasi–two-dimensional (2D) electron or hole gas becomes quantized with values $R_{xy} = h/e^2j$ (where h is Planck's constant, e is the electron charge, and j is an integer), has been observed in a variety of inorganic semiconductors, such as Si, GaAs, InAs, and InP. At higher magnetic fields, fractional quantum Hall states where j is not an integer have also been observed (*2*). A QHE-like state was also seen in organic materials such as Bechgaard salts $(TMTSF)_2X$ (where TMTSF is tetramethyl tetraselenafulvalene and X = ClO_4, ReO_4, or PF_6) (*3–5*). However, in these materials the QHE is related to a series of field-induced spin density wave transitions (*5*) to states with filled Landau bands (*6*). We report on the observation of the integer and fractional QHE in a 2D electron and hole gas in the organic semiconductors tetracene and pentacene. This was achieved in a 2D electron-hole system generated in a single crystal–based MIS device.

Pentacene and tetracene single crystals were grown from the vapor phase in a stream of flowing gas (*7, 8*). The resulting high-quality single crystals support ambipolar (i.e., electron and hole) transport (*9*). Thermally evaporated gold films provide ohmic contacts for holes as well as electrons. Because these crystals are of high resistivity ($>10^{14}$ ohm·cm), the charge carriers must be injected in a field-effect transistor geometry, in which an Al_2O_3 layer (capacitance ~130 nF cm^{-2}) serves as the gate dielectric. A thin gold layer is deposited as the gate electrode on top of the structure. We can then produce a 2D electron or hole gas, respectively, in the channel region of an organic field-effect transistor (*10*), with the carrier density controlled by the gate bias.

The charge transport properties in these

Bell Laboratories, Lucent Technologies, 600 Mountain Avenue, Murray Hill, NJ 07974, USA.